

VIP Very Important Paper

# Corrosion-Free EMF Measurements of Zinc-Based Intermetallic Compounds at Ambient Temperature

René Kriegel<sup>[a]</sup> and Marc Armbrüster<sup>\*[a]</sup>

Material development requires in many cases information about the necessary stability of the materials against oxidation, which is encoded in the chemical activity of the constituting elements. Determination of the chemical activity is tedious, especially for metallic materials at or close to ambient temperature. To determine the chemical activity of Zn at ambient temperature, electromotive force (EMF) measurements on the intermetallic compounds ZnPd, ZnPt and Cu<sub>5</sub>Zn<sub>8</sub> within their respective homogeneity range were conducted. The single-phase nature of the samples was confirmed by powder X-ray diffraction, light microscopy as well as SEM/EDX analysis. To exclude oxidation, and therefore faulty determination of the electrochemical potentials, a method was developed to conduct the electro-

chemical measurements under non-corrosive conditions in inert atmosphere. Corrosion by the electrolyte was avoided using anhydrous dimethylformamide as aprotic solvent. From the EMF the respective intrinsic activities of zinc in the corresponding intermetallic compounds was determined. Measurements on Cu<sub>5</sub>Zn<sub>8</sub> and comparison to available data in literature verified the developed method allowing to retrieve thermodynamic data of ZnPd and ZnPt for the first time at ambient temperature. The herein developed and easy-to-use methodology is applicable to a wide range of metallic material by choosing appropriate compositions of the electrolyte and has the potential to boost material development.

## 1. Introduction


Although efforts towards a knowledge-based understanding of heterogeneously catalyzed processes have steadily increased in recent decades, the traditional development and optimization of catalysts is in most cases still based on empirical and fact-based values.<sup>[1]</sup> This empirical approach in the search for better catalyst materials is greatly accelerated by techniques such as high-throughput screening, in which variations of thousands of potential catalyst materials can be investigated concerning their catalytic activity within a very short time.<sup>[2,3]</sup> Although the success of such methods and the associated justification for their existence cannot be denied, there is still the possibility that promising materials are overlooked by such a screening.


Due to their ordered crystal structure and their low affinity to segregation, intermetallic compounds are particularly suitable for use in the field of knowledge-based catalytic investigations.<sup>[4]</sup> The above-mentioned characteristic properties of intermetallic compounds ensure a reproducibility of defined surface structures and thus a direct correlation between the catalytic behavior and the crystal and/or electronic structure of

an intermetallic compound.<sup>[5]</sup> The formation of partially very broad homogeneity ranges of the intermetallic compounds (realized by substitution, filling of interstitial spaces of the surplus type of atom or by voids of the subordinate type of atom) also offer the possibility of changing the electronic structure of an intermetallic compound while largely retaining the geometric structure, whereby a separate analysis of the influence by changing the electronic structure of an intermetallic compound becomes accessible. The enormous potential of intermetallic compounds for knowledge-based catalysis research is illustrated by examples such as the development of non-precious metal catalyst materials for the semi-hydrogenation of acetylene,<sup>[6]</sup> the development of stable and highly active catalysts for methanol steam reforming (MSR)<sup>[7]</sup> as well as their broad use in electrocatalysis.<sup>[8]</sup> Interest has been high concerning the intermetallic compounds in the Pd–Zn system. While ZnPd aided deep understanding in MSR<sup>[9]</sup> as well as methanol synthesis<sup>[10]</sup> and the semi-hydrogenation,<sup>[11]</sup> compositions in the  $\gamma$ -phase region have been successfully tested concerning their properties in the electrochemical oxygen reduction.<sup>[12]</sup>

The classification of compounds with respect to their potential catalytic properties can be done with the aid of universal material parameters, which allow a chain connection between a material and its catalytic behavior.<sup>[13]</sup> An example for the connection between catalytic behavior and prevailing thermodynamic conditions of a material is the Brønsted-Evans-Polanyi relationship, which postulates a linear dependency between the activation energy and the change of enthalpy regarding elementary reaction steps.<sup>[14,15]</sup> Such dependencies can also be extended by a quantitative understanding through the concept of scaling relationships developed by Nørskov et al.<sup>[16]</sup>

[a] Dr. R. Kriegel, Prof. Dr. M. Armbrüster  
Faculty of Natural Sciences, Institute of Chemistry  
Materials for Innovative Energy Concepts  
Technische Universität Chemnitz  
Straße der Nationen 62, 09107 Chemnitz, Germany  
E-mail: marc.armbruester@chemie.tu-chemnitz.de

 Supporting information for this article is available on the WWW under <https://doi.org/10.1002/cphc.201901218>

 © 2020 The Authors. Published by Wiley-VCH Verlag GmbH & Co. KGaA. This is an open access article under the terms of the Creative Commons Attribution Non-Commercial License, which permits use, distribution and reproduction in any medium, provided the original work is properly cited and is not used for commercial purposes.

The change in the observed enthalpy values of two materials can be traced back to the different chemical potentials of the corresponding materials. In theory, the chemical potential can be used as a superordinate material constant to describe the reactivity of a system. Knowledge of the chemical potential of a system thus opens up the possibility of formulating predictions regarding its reactivity with other systems<sup>[17]</sup> or reactive atmospheres, also comprising its catalytic behavior. The use of the chemical potential or activity, which is directly linked with the chemical potential of a material or a component of a material, respectively, as an indicator in heterogeneous catalysis is advantageous because these parameters combine several factors relevant for the catalytic behavior and thus simplify trend predictions in a clear manner. This has already been clearly demonstrated in quantum chemical investigations regarding the kinetics of heterogeneously catalyzed reactions.<sup>[18]</sup>

A very exact method for the determination of activity values and free enthalpies in metallic multi-component systems is the measurement of the electromotive force (EMF) between the system to be investigated and its non-precious component.<sup>[19]</sup> The principle for this analysis method results from the fact that in a galvanic cell of the structure  $A | A^{z+}$  (ionic conductor)  $| A_x B_{1-x}$  the EMF is directly linked to the partial molar free enthalpy of mixing of component A in the multi-component system and its activity  $a_A$  via the relationships:

$$\Delta \bar{G}_A = R \cdot T \cdot \ln a_A \quad (1)$$

and

$$\Delta \bar{G}_A = -z \cdot F \cdot \Delta E_A \quad (2)$$

By converting Equation (1) to  $\ln a_A$  and replacing the partial molar free enthalpy by the relationship shown in Equation (2), it becomes obvious that the activity value at constant temperature can be determined from the electrode potential as follows [Eq. (3)]:

$$\ln a_A = -\frac{z \cdot F \cdot \Delta E_A}{R \cdot T} \quad (3)$$

Purified eutectic salt melts, e.g. LiCl/KCl,<sup>[20]</sup> or solid state electrolytes such as doped ZrO<sub>2</sub> anion conductors<sup>[21]</sup> are mostly used as electrolytes for the performance of EMF measurements on metallic systems. Both types of electrolyte are characterized by the fact that temperatures around 700 K must prevail in order to ensure a sufficiently high conductivity. Other methods for thermodynamic analyses of solids (e.g. calorimetry and vapor pressure measurements<sup>[22]</sup>) are also conducted at high temperature. If the electrolyte is selected appropriately, EMF measurements can also be carried out at or close to ambient temperature. This e.g. allows phase diagram investigations to be extended to lower temperature ranges<sup>[23]</sup> as well as to investigate materials in a temperature range in which they are usually used for heterogeneously catalyzed reactions.

When measuring EMF using an electrolyte that is liquid at ambient temperature, it should be noted that even minor surface changes – caused by corrosion – have a considerable influence on the resulting cell voltage. To avoid falsification of the measurement results by the formation of mixing potentials, the electrochemical potential measurements must be carried out under non-corrosive conditions. Ambient temperature measurements are therefore mainly carried out in an inert gas atmosphere and by using a non-aqueous electrolyte. The use of solvents such as isopropyl alcohol or propylene carbonate, which were dried before use and dewatered by pre-electrolysis over several days, did not completely prevent surface corrosion in previous investigations.<sup>[24,25]</sup> Thus, an estimation of the electrochemical potential of compounds, which tend to surface corrosion, is so far only possible by the constant generation of new surfaces in connection with corrections for corrosion.<sup>[24,25]</sup>

The aim of this work is the development of a method for the determination of activity values from EMF measurements under non-corrosive conditions at ambient temperature. In addition, activity values of the intermetallic compounds ZnPd and ZnPt were determined for the first time using the corresponding method. In order to investigate the influence of the activity values of zinc in the intermetallic compounds ZnPd and ZnPt depending on the electronic structure, single-phase compounds with different zinc contents were tested within the homogeneity range. Due to their proven oxidation sensitivity, investigations on zinc-rich ZnPd are also particularly suitable for testing the designed methodology (i.e. for verifying whether EMF measurements at ambient temperature on corrosion-sensitive materials are accessible). To validate the developed method, Cu<sub>5</sub>Zn<sub>8</sub> was investigated, for which composition-dependent EMF reference values at ambient temperature are available.<sup>[25,26]</sup>

## Experimental Section

### Synthesis

For the preparation of intermetallic electrodes of Cu<sub>5</sub>Zn<sub>8</sub>/ZnPd/ZnPt Cu-foils (Alfa Aesar, 99.999%, thickness: 0.1 mm)/Pd-foils (ChemPur, 99.9%, thickness: 0.25 mm)/Pt-foils (ChemPur, 99.99%, thickness: 0.1 mm), each with a width of roughly 1 cm and a length of up to 2.5 cm, and zinc granules (Alfa Aesar, 99.9999%, diameter: 1–6 mm) were used to obtain samples in the form of foils.<sup>[27]</sup> The weighted reactants were evacuated and sealed in quartz glass ampoules avoiding direct contact of the zinc granules and the corresponding foil by means of a neck. The evacuated tubes were placed upright in a furnace and heated to 450 °C with 60 Kh<sup>-1</sup>, held for one day, before heating to 720 °C (for the preparation of Cu<sub>5</sub>Zn<sub>8</sub>-foils), or 900 °C (for the preparation of ZnPd- and ZnPt-foils) with 60 Kh<sup>-1</sup> followed by 10 to 90 days of annealing. After reaction of the vaporized Zn and the corresponding foils, the ampoules were cooled down to 40 °C with 5 Kh<sup>-1</sup> (in the case of Cu<sub>5</sub>Zn<sub>8</sub>-foils) or quenched in water (in the case of ZnPd- and ZnPt-foils). No interactions of the reactants with the quartz glass were observed.

## Characterization

Powder X-ray diffraction (XRD) patterns (Huber image plate G670, Cu  $K\alpha_1$ ,  $\lambda=1.54056 \text{ \AA}$ , curved germanium (111) monochromator,  $3^\circ < 2\theta < 100^\circ$ ) were recorded to verify the single-phase nature of the intermetallic electrodes.

The elemental compositions of the intermetallic electrodes were determined by weighing the starting materials (i.e. the corresponding Cu-/Pd-/Pt-foil and the zinc granules) before the vapor-solid-reaction of zinc and metal foil took place and the resulting intermetallic foil after the reaction. From the difference between the two masses, the elemental composition can be given with an accuracy of at least  $\pm 0.1 \text{ at.}\%$ . Elemental composition of the samples was also partially verified by inductively coupled plasma – optical emission spectrometry (ICP-OES 5100, Agilent Technologies). For this purpose, the samples were dissolved in aqua regia and analyzed in triplicate. All elemental analyses were evaluated by matrix-matched calibrations.

To validate the single-phase nature of the produced intermetallic foils, both metallographic sections of the surfaces and cross sections were prepared and examined by light microscopy. To produce the metallographic sections, the samples were embedded either hot or cold before polishing. Light micrographs of metallographic sections of the intermetallic electrodes were taken on a Zeiss Axioplan 2.0 in bright field as well as under polarized light.

Scanning electron microscopy (SEM) and energy-dispersive X-ray spectroscopy (EDX) of metallographically prepared sections were carried out on a JEOL JSM-7800F between 20 and 25 keV.

## EMF Measurements

For the conduction of the EMF measurements a method was developed, which allows measurements on corrosion-sensitive, brittle intermetallic compounds. The EMF measurements were generally carried out in a glove box with argon atmosphere ( $\text{H}_2\text{O}$  and  $\text{O}_2 < 0.1 \text{ ppm}$ ). To contact the electrodes inside the glove box with the potentiostat (SP-200, BioLogic) located outside, a vacuum-tight plug, to which four-core cables one meter long were soldered on both sides, was cast into a vacuum flange and mounted on the glove box. The contact between the vacuum-tight plug and the potentiostat was made via banana plugs. The electrodes inside the glove box were contacted with crocodile clips. The evaluation of the measurement results was carried out with the software EC-Lab from BioLogic.<sup>[28]</sup>

The restricted mobility in a glove box required a measurement setup that allowed easy handling of the experiments. A method for renewing the electrode surfaces before the start of the EMF measurements had to be implemented in which simultaneous breaking of the thin intermetallic foils could be avoided. These requirements led to the development of the polishing machine shown in Figure 1. The size of the polishing machine is such that it can be inserted through the large antechamber of the glove box used, i.e. without prior disassembly. The polishing machine is equipped with a motorized rotating polishing plate. The rotation speed of the polishing plate can be continuously adjusted by a speed control on the front of the polishing machine. The polishing disc itself is made of polyetheretherketone (PEEK).

The polishing disc is fixed to the motor axis with a grub screw. This allows a quick assembly/disassembly and thus a quick exchange of the polishing plates between two experiments. The diameter of the polishing plate (76 mm) has been designed so that commercially available self-adhesive polishing wheels can be used as grinding-media. SiC paper (Buehler Carbimet P600) was preferred.

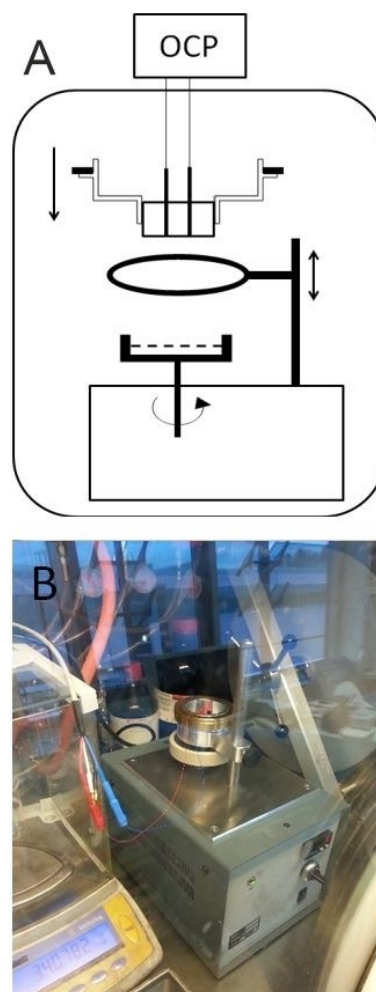


**Figure 1.** Experimental setup for the EMF measurements. A) Schematic of the setup. B) Position of the polishing machine in the glove box with contacted electrodes.

To renew the electrode surfaces, the foils were first fixed upright in embedding material (epoxy resin adhesive, UHU plus endfest 300). The embedding served to mechanically stabilize the electrodes, which prevented the intermetallic foils from breaking during the polishing process. In addition, the electrodes were embedded in a fixed position, which avoided any short-circuits during the EMF measurements. The upper part of each electrode was excluded from the embedding to ensure contact by crocodile clips (see Figure S1 in the Supporting Information). For surface renewal, the puck with the embedded foils was fixed in a self-constructed aluminum holder with four grub screws in such a way that part of it protruded below the aluminum holder. In an appropriate guide, which was attached to a height-adjustable guide rod, the aluminum holder could be lowered in a controlled manner onto the polishing plate until the weight of the aluminum holder rested on the polishing plate. The weight force acting on the electrodes during the polishing process could be adjusted via brass rings made of varying masses.

EMF measurements were carried out by fixing the zinc-based intermetallic foils together with a piece of zinc foil (ChemPur, 99.99%, thickness: 0.5 mm) of approximately the same dimensions at a distance of 1 to 1.5 cm between each other in embedding material. To exclude an oxidative influence of air bubbles trapped

in the embedding material during the polishing process, the embedding was carried out in the glove box.

After embedding the foils, they were first polished by hand in the glove box using  $\text{Al}_2\text{O}_3$  grinding paper (VSM, 320 brown body KK 114F). Afterwards, the embedded foils were cleaned of grinding residues with a paper towel and fixed in the aluminum holder. The electrolyte was also prepared directly before the measurements in the glove box (zinc salt, conducting salt, electrolyte solvent). It was placed in a flat Petri dish on the polishing machine and the aluminum holder was lowered over the guide rod until the underside of the embedded foil pieces was immersed in the electrolyte. After the first measurement period was finished, the embedded foils were guided onto the polishing plate equipped with polishing paper and the undersides were polished for a few seconds to a few minutes at an average speed of the polishing device (roughly 200 rpm). The conducted polishing served to renew the electrode surfaces and/or to disturb the previously detected potential value. Afterwards, the underside was again cleaned of grinding residues with a paper towel and a new measurement period was carried out. This process was optionally repeated several times. Thus, OCP measurements were not carried out during polishing, but started directly after the polishing events. The achievement of the same potential value before and after mechanical disturbance was interpreted as a sufficient condition for the observation of an equilibrium potential.

## 2. Results and Discussion

### 2.1. Synthesis and Characterization

Foils of the intermetallic compounds ZnPd, ZnPt and  $\text{Cu}_5\text{Zn}_8$  with different elementary compositions were synthesized, which allowed direct usage as electrode. Phase compositions were determined by powder X-ray diffraction (XRD). As shown in Figures S2–S4, only the corresponding intermetallic compounds could be detected in all samples directly after synthesis. The elementary compositions shown in Figures S2–S4 were (if possible) determined by the weighing method as described above. The elementary compositions in Figure S4, which are indicated with standard deviations, were determined from ICP-OES measurements. In these cases, it was not possible to determine the composition by weighing due to breaking of the foils while opening the quartz glass ampoules. Light micrographs (Figures S5 and S6) and SEM/EDX analyses (Figures S7 and S8) from polished ZnPt and  $\text{Cu}_5\text{Zn}_8$  electrodes revealed only one phase as well, thus confirming the single-phase status. Furthermore, the EDX analyses of also reveal a homogeneous distribution of zinc and platinum/copper over the entire thickness of the foil. Morphology and single-phase status of intermetallic ZnPd foils with varying elementary composition synthesized by vapor-solid reaction were already analyzed and discussed in the course of earlier examinations. In this respect, we refer to the studies of Ivarsson et al.<sup>[27]</sup>

### 2.2. Methodology Development

The aim of the methodology development was to establish a reliable, quick and cheap procedure for EMF measurements on

corrosion-sensitive binary intermetallic compounds. Since the intermetallic foils to be investigated potentiometrically were stored in air, the first challenge was to create an oxide-free surface layer. In earlier studies, this was achieved by moving a rotating working electrode towards a grinding wheel or by breaking the electrode in the electrolyte.<sup>[24]</sup> Both methods for surface renewal were not considered in the present case. The use of a rotating working electrode requires the presence of a compact intermetallic regulus from which a circular disk electrode can be made. In addition, the design effort for the production of a corresponding measurement setup is considerable. The breaking of the intermetallic foils would be possible, but due to the existing lengths of the foils and the high brittleness it would in most cases only allow a single measurement or would involve the risk of uncontrolled breaking of the foils into many individual parts. Due to the high experimental effort required for the production of the single-phase intermetallic foils, a less destructive method of surface renewal was sought, which allows both measurements under continuous new generation of surface and multiple measurements on a sample. The solution for these requirements was a partial embedding of the working and counter electrodes at a defined distance from each other. The fixation of the electrodes in the embedding medium allowed the polishing of the electrode surfaces relevant for the potential measurements and at the same time prevented the breakage of the intermetallic foils. The non-embedded sides of the electrodes also allowed simple contacting with crocodile clips.

The electrolyte for the measurements had to be primarily non-aqueous in nature, liquid at ambient temperature, preferably highly conductive and containing zinc ions as charge carriers. As a secondary aspect, low toxicity was taken into account when selecting the electrolyte. Since earlier studies had shown that protic solvents such as isopropanol may prevent the measurement of corrosion-free potentials,<sup>[24]</sup> this substance class was not further considered. In addition to aprotic solvents, ionic liquids appeared interesting for use as electrolyte solvents due to their intrinsic ionic character and their low vapor pressure.<sup>[29]</sup> However, due to the generally high viscosity of ionic liquids<sup>[30]</sup> and the fact that at least commercially available ionic liquids always contain, in addition to a residual amount of water, other partially unknown impurities, which can vary greatly in type and amount per batch,<sup>[31]</sup> extensive testing of ionic liquids as electrolyte solvents was avoided. In preliminary tests with the ionic liquid 1-butyl-1-methylpyrrolidinium-bis(trifluoromethylsulfonyl)imide (BMP-BTI, Sigma Aldrich,  $\geq 98.5\%$ ) it was revealed, that the inadequate solubility of zinc salts – the solubility of both zinc bis(trifluoromethylsulfonyl)imide ( $\text{Zn}(\text{NTf}_2)_2$ , Sigma Aldrich, 95%) and  $\text{ZnCl}_2$  (Sigma Aldrich,  $\geq 98\%$ ) was tested – also represents a problem in the use of ionic liquids as electrolyte solvents.

In favor of a precisely defined electrolyte of manageable complexity, the aprotic, polar solvent N,N-dimethylformamide (DMF, Sigma Aldrich, 99.8%) was selected as electrolyte solvent. DMF is commercially available in anhydrous form ( $\text{H}_2\text{O} < 50$  ppm), has excellent dissolving properties for a variety of metal salts even in anhydrous form and is classified as non-

acutely toxic according to GHS labelling. In addition, the electrochemical stability of DMF has already been demonstrated in applications such as electrolytic capacitors and the electrochemical production of corrosion-sensitive intermetallic compounds.<sup>[32,33]</sup> In contrast to, e.g., propylene carbonate,<sup>[24]</sup> DMF has thus already demonstrated to be non-corrosive towards corrosion-sensitive compounds. Accordingly, with the epoxy resin "UHU plus endfest 300" (binder:hardener ratio of 2:1) an embedding material was used for fixation of the electrodes, which exhibits a high chemical resistance to DMF.

High-purity, anhydrous zinc chloride (Sigma Aldrich,  $\geq 99.995\%$ ) was selected as the zinc salt and lithium chloride (Sigma Aldrich, 99.998%) was added to the electrolyte as conducting salt in likewise high-purity, anhydrous state. The use of zinc sulfate (Sigma Aldrich,  $\geq 99.9\%$ ) as zinc salt and lithium perchlorate (Sigma Aldrich, 99.99%, battery grade) as conducting salt was also successfully tested. However, due to the lower ion mobility and the associated longer time required to achieve equilibrium of the potential values, the use of  $\text{ZnSO}_4$  or  $\text{LiClO}_4$  was generally avoided. For the electrolyte used in the EMF measurements a concentration of 0.5 M  $\text{ZnCl}_2$  and 1 M LiCl (optimized with regard to electrolyte conductivity) was generally adjusted.

### 2.3. Validation of the Developed Methodology

The validation of the developed methodology was carried out by EMF measurements on intermetallic electrodes of  $\text{Cu}_5\text{Zn}_8$ , which have been already extensively investigated. Based on EMF measurements on  $\text{Cu}_5\text{Zn}_8$  and subsequent comparison with experimental reference values from earlier studies, statements could be made regarding the correct size range of the obtained potential values.

In this respect, the aim was to derive the underlying relationships to existing ambient-temperature reference data, which should facilitate the verification of the own results in the further process. Due to the large number of publications, the two-component-system Cu–Zn is suitable as a reference system for thermodynamic investigations. Figure 2 summarizes experimentally determined electrode potentials for various Cu–Zn ratios at different temperatures.

The vertical lines delimit the homogeneity range of  $\text{Cu}_5\text{Zn}_8$  at 720 °C. The electrochemical potential of zinc in the binary mixture decreases with increasing zinc content. The potential decrease is not linear, but reveals several plateaus and potential gradients with different slopes. The potential gradient correlates with the prevailing single-phase and two-phase regions. Plateaus in this context indicate the presence of a two-phase area, whereas gradients indicate single-phase areas. Taking into account the existing reference data, an initial assessment of the own measured values can be carried out. The equilibrium potential values of the synthesized  $\text{Cu}_5\text{Zn}_8$  samples show the expected gradual decrease of the potential with increasing zinc content ( $\Delta E_{\text{Zn}}$ :  $\text{Cu}_{38.1(1)}\text{Zn}_{61.9(1)} = 35.0(1)$  mV,  $\text{Cu}_{34.0}\text{Zn}_{66.0} = 24.7(5)$  mV,  $\text{Cu}_{33.4(2)}\text{Zn}_{66.6(1)} = 12.4(8)$  mV). Comparison to ambient-temperature measurements on compounds with similar

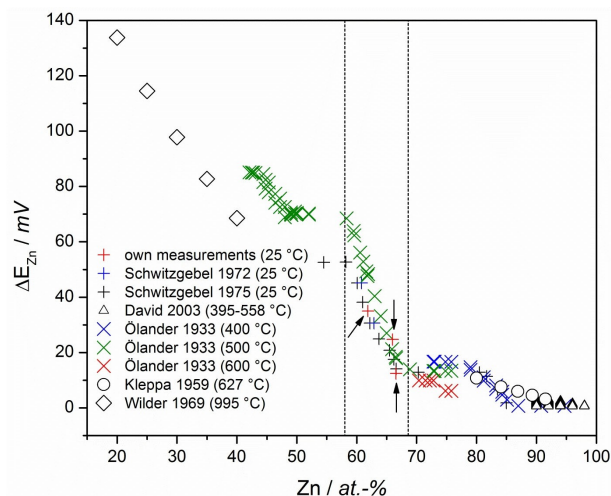


**Figure 2.** Own equilibrium potentials of the  $\text{Cu}_5\text{Zn}_8$  electrodes determined from EMF measurements in comparison to reference data.<sup>[25,26, 34–37]</sup> The equilibrium potentials are plotted against atomic percent zinc. The vertical dashed lines indicate the limits of the homogeneity range from the  $\text{Cu}_5\text{Zn}_8$  phase at 720 °C based on the most recent phase diagram.<sup>[38]</sup> The inserted arrows serve the better identification of our values. The standard deviations of the values obtained in this study lie within the point expansions.

composition<sup>[25,26]</sup> reveals an excellent agreement, thus indicating the correctness of our measurements. Comparing data gathered at different temperatures, no general trend is discernible (Figure 2). For example, the investigations of Ölander on compounds with the same composition show a decrease of the zinc potential in the binary compound when the temperature increases.<sup>[35]</sup> Comparable measurements by David et al. on compounds of the Cu–Zn system with a higher zinc content, however, show the opposite behavior.<sup>[34]</sup> This may be explained by the fact that the measured electrode potentials depend on two variables, namely the temperature and the activity of the individual components, which do not necessarily have to show a proportional correlation.

After the assessment of the electrode potentials of zinc in the binary Cu–Zn system, the activity values of zinc in the phase system were derived according to eq. (1) and resulted in activity values of  $\ln a_{\text{Zn}} \text{Cu}_{38.1(1)}\text{Zn}_{61.9(1)} = -2.73(1)$ ,  $\text{Cu}_{34.0}\text{Zn}_{66.0} = -1.92(4)$  and  $\text{Cu}_{33.4(2)}\text{Zn}_{66.6(1)} = -0.97(6)$ . Since the activity values allow a direct comparison of thermodynamic data collected by different analytical methods, the available data for the Cu–Zn system are summarized in Figure 3. The Raoult line serves as reference for the activity values of an ideal binary solution.

Comparison of the experimentally determined values for  $\ln a_{\text{Zn}}$  with the Raoult line shows that the fit between the two increases when the zinc content or the temperature increases. This behavior can be brought into line with theoretical considerations. With increasing zinc content the general approximation to the activity value for elementary zinc ( $\ln a_{\text{Zn}} = 1$ ) is to be expected. At the same time, the atomic mobility in the lattice is increased by increasing the temperature, which causes decreasing interatomic interactions and results in an approximation of the activity values to ideal solution behavior.

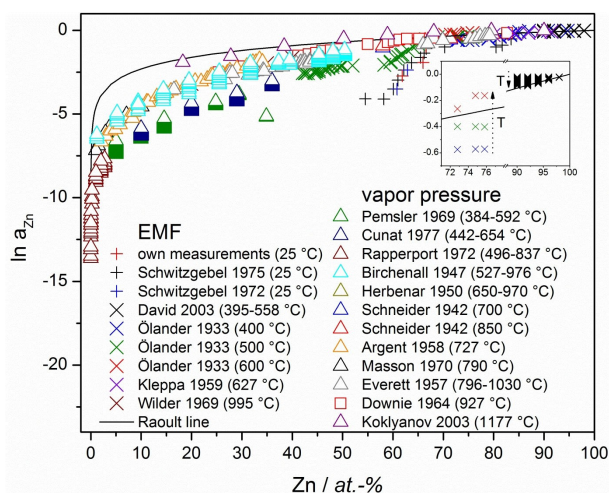


**Figure 3.** Illustration of experimental activity values for zinc in the Cu–Zn system.<sup>[25,26, 34–37, 39–49]</sup> The activity values are logarithmically plotted against atomic percent zinc. The standard deviations of the own measured values lie within the point expansions. Inset: temperature-dependent change of the activity values of Ölander and David et al.<sup>[34,35]</sup>

In the presence of metal melts, the correlation between real and ideal activity values is therefore at its greatest (see, for example, Koklyanov<sup>[49]</sup>). Considering the Raoult line as reference point, the opposite temperature-potential profiles of the investigations of Ölander and David et al. can also be explained. The inset of Figure 3 shows that the activity values between 70 and 80 at.% zinc are below the Raoult line, while the ones between 90 and 98 at.% zinc are above. Activity values below the Raoult line indicate an exothermic mixing enthalpy of the binary solution.<sup>[50]</sup> Put simply, this means in the concrete case of the Cu–Zn system that there is a stronger bonding between copper and zinc atoms than between atoms of the same type of element. The atoms thus strive to have one atom of the other element as their closest neighbor, which leads to ordering phenomena and a tendency towards the formation of intermetallic compounds. In contrast, activity values above the Raoult line are equivalent to the presence of an endothermic enthalpy of mixing. The resulting stronger binding energies between atoms of the same type are a clear indication for cluster formation and segregation within the (solid) solution. When a temperature increase occurs, the activity values from different sides approach the Raoult line and consequently the ideal solution behavior. The approach from different sides of the Raoult line leads simultaneously to the observation of opposite potential curves at a temperature change. Based on this knowledge, it is therefore not surprising that the activity values determined at ambient temperature deviate most strongly from the ideal behavior, since in this case the thermodynamic urge to form an intermetallic compound is most clearly demonstrated by the pronounced interatomic interactions.

For many bimetallic systems, no thermodynamic data is available close to ambient temperature. Thus, it is necessary to derive the temperature-dependence of the activity values to

allow for comparison of our values to high-temperature data. Here, an approximation is possible by adopting the Gibbs-Helmholtz equation [Eq. (4)]:

$$\left(\frac{\partial(\Delta\bar{G}_{Zn}/T)}{\partial(1/T)}\right)_p = \Delta\bar{H}_{Zn} \quad (4)$$

wherein  $\Delta\bar{H}_{Zn}$  stands for the partial molar enthalpy of mixing of zinc in the bimetallic system and  $\Delta\bar{G}_{Zn}$  stands for the partial molar free enthalpy (Gibbs energy) of mixing of zinc in the bimetallic system.

Assuming finite changes and applying the relationships [Eqs. (5) and (6)]

$$\Delta\left(\frac{1}{T}\right) = \frac{1}{T_2} - \frac{1}{T_1} \quad (5)$$

and

$$\Delta\left(\frac{\Delta\bar{G}_{Zn}}{T}\right) = \frac{\Delta\bar{G}_{Zn, T_2}}{T_2} - \frac{\Delta\bar{G}_{Zn, T_1}}{T_1}, \quad (6)$$

the Gibbs-Helmholtz equation can be transformed as follows [Eq. (7)]:

$$\frac{\Delta\bar{G}_{Zn, T_2}}{T_2} - \frac{\Delta\bar{G}_{Zn, T_1}}{T_1} = \Delta\bar{H}_{Zn} \cdot \left(\frac{1}{T_2} - \frac{1}{T_1}\right). \quad (7)$$

Taking into account the relationship [Eq. (8)]

$$\Delta\bar{G}_{Zn} = R \cdot T \cdot \ln a_{Zn}, \quad (8)$$

the partial molar free enthalpy  $\Delta\bar{G}_{Zn}$  can now be replaced by the activity value of zinc. By converting the equation obtained in this way, the partial activity at a second variable temperature is accessible [Eq. (9)]:

$$\ln a_{Zn, T_2} = \frac{\Delta\bar{H}_{Zn}}{R} \cdot \left(\frac{1}{T_2} - \frac{1}{T_1}\right) + \ln a_{Zn, T_1} \quad (9)$$

The application of the formalism derived above requires the knowledge of the partial molar enthalpy and therefore cannot be applied to all known data sets. In the case of the thermodynamic investigations of Cunat et al.,<sup>[40]</sup> Downie,<sup>[48]</sup> and Koklyanov et al.<sup>[49]</sup> on the Cu–Zn system, partial molar enthalpies were determined, allowing the application of the derived formalism. Figure 4 shows the zinc activity values converted to ambient temperature compared to the original experimental data and activity values determined from EMF measurements at ambient temperature.

As a tendency, the expected decrease of the zinc activity values becomes clear when applying the approximate calculation to ambient temperature, which at the same time leads to a larger gap between the Raoult line and the zinc activity values. In comparison with the original data, the values converted to ambient temperature also show a clearer expression of plateaus and gradients in the activity profile with

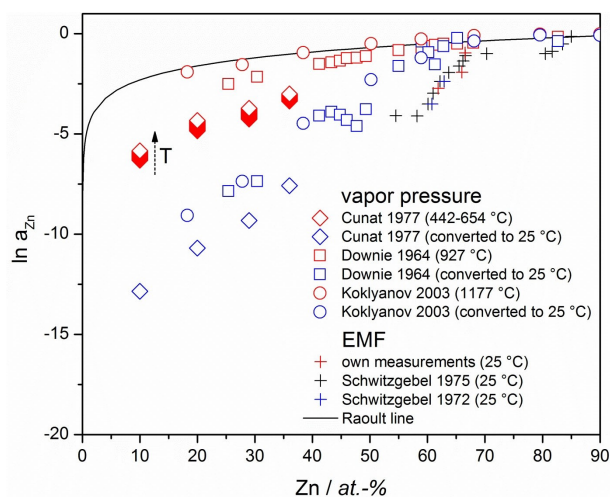


**Figure 4.** Calculated approximation of high temperature activity values from the Cu–Zn system<sup>[40,48,49]</sup> to ambient temperature and comparison with experimental values determined at ambient temperature.<sup>[25,26]</sup> The standard deviations of the values derived in this study lie within the point expansions.

a change in the zinc content. Activity values, determined at different temperatures, occupy the same size range after conversion to ambient temperature. Thus, the temperature-dependent measurements of Cunat et al. after ambient temperature conversion are reduced to exactly one activity value per composition. When applying the approximate calculation to different data sets, it becomes clear that an exact agreement of the converted activity values is not always given. The lack of an exact agreement between converted and experimental ambient temperature activity values can be explained by the obviously wide scatters of the partial molar enthalpy values used, which can differ by several kilojoules per mole depending on the reference used at otherwise comparable elementary composition. In addition, an influence of measurements in the melt compared to solid-state measurements cannot be excluded.

The adoption of activity values from literature to ambient temperature allows comparison to our data and, thus, further validating our EMF ambient temperature measurements. Due to the strong scattering of the available partial molar enthalpy values, a comparison to the derived ambient-temperature values can only serve as a confirmation of the order of magnitude of the measured activity values.

## 2.4. EMF Measurements on Intermetallic ZnPd Electrodes

To determine the equilibrium values for the ZnPd electrodes with varying elemental composition, several EMF measurements in the optimized electrolyte 0.5 M ZnCl<sub>2</sub>/1 M LiCl/DMF were conducted and resulted in very different potentials for the investigated compositions (Figure 5). Already at the beginning of the EMF measurements, all three electrodes show stable potentials of Zn<sub>44.0</sub>Pd<sub>56.0</sub> = 502(1) mV, Zn<sub>49.9</sub>Pd<sub>50.1</sub> = 402(8) mV and Zn<sub>52.0</sub>Pd<sub>48.0</sub> = 82.7(2) mV, which differ markedly from each other. After disturbance of the potential measurements by

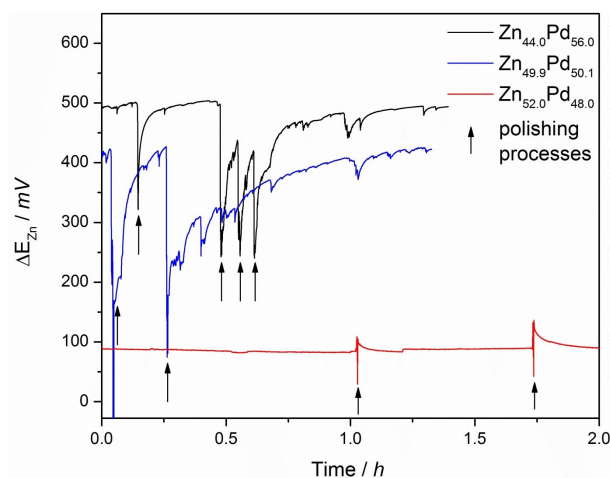


**Figure 5.** EMF measurements on Zn<sub>44.0</sub>Pd<sub>56.0</sub>, Zn<sub>49.9</sub>Pd<sub>50.1</sub> and Zn<sub>52.0</sub>Pd<sub>48.0</sub> in inert gas atmosphere by using 0.5 M ZnCl<sub>2</sub>/1 M LiCl/DMF as electrolyte. In each case, the electrode surfaces were renewed before the measurements were started.

polishing (arrows in Figure 5), the potential values need a few minutes to about half an hour to return to the original value. It is noticeable that Zn<sub>44.0</sub>Pd<sub>56.0</sub> and Zn<sub>49.9</sub>Pd<sub>50.1</sub> approach the original value from lower potentials, while Zn<sub>52.0</sub>Pd<sub>48.0</sub> approaches the original value from higher potentials.

The striving for the initial stable potential value after the disturbance is reproducible, indicating that these values represent equilibrium potentials. The change of the equilibrium potential of the ZnPd electrodes as a function of the elemental composition corresponds qualitatively to the expected trend. Since no measurements at ambient-temperature are known for this material, the correctness of the obtained potentials cannot be directly verified. However, it can be assumed that the found equilibrium potentials are not influenced by corrosion. In previous reference measurements on ZnPd electrodes in air, i.e. under corrosive conditions, it was observed that mixing potentials of ZnPd electrodes are located in potential ranges of more than one volt (potential measurements on Zn<sub>44.0</sub>Pd<sub>56.0</sub> in air led to a reproducible potential value of 1.1 V). Corrosion of the intermetallic electrodes would also result in an increase of the potential value over time. Since investigations on the electrode Zn<sub>52.0</sub>Pd<sub>48.0</sub>, which is richest in zinc and therefore most sensitive to corrosion, reveal a rather opposite potential profile after disturbance of the equilibrium, the measuring conditions can generally be regarded as non-corrosive. Why the electrodes in dependence of the zinc content obviously approach the equilibrium potential from different sides after the disturbance has occurred cannot be completely clarified on the basis of the available results. It is conceivable that the different approach to the equilibrium potential is associated with a different mechanism. This could be due to differences in zinc segregation caused by the different occupation of crystallographic positions depending on the elemental composition, i.e. mixed occupancy to realize the different compositions.<sup>[27]</sup> The fluctuations in the potential profile without conscious external influence show the

sensitivity of the equilibrium, which can apparently be disturbed by the smallest internal and external influences (concentration gradients in the electrolyte, temperature fluctuations, vibrations, light shocks, ...). Since a negative influence of the chloride ions on the measurements could be expected (e.g. conceivable by complex formation/leaching of the palladium contained in the electrodes), measurements were repeated in chloride-free electrolytes ( $\text{ZnSO}_4$  as zinc salt,  $\text{LiClO}_4$  as conducting salt) or electrolytes without conducting salt. No significant differing potentials were obtained, thus excluding an influence of lithium or chloride ions on the determined potentials.

The determined potential values and calculated zinc activity values ( $\ln a_{\text{Zn}}$ :  $\text{Zn}_{44.0}\text{Pd}_{56.0} = -39.10(9)$ ,  $\text{Zn}_{49.9}\text{Pd}_{50.1} = -31.3(6)$ ,  $\text{Zn}_{52.0}\text{Pd}_{48.0} = -6.44(2)$ ) are compared to literature values, which

were determined on the basis of vapor pressure measurements (Figure 6). In addition, the activity values determined by Chiang et al. at  $1000^\circ\text{C}$ <sup>[51]</sup> were converted to ambient temperature and the corresponding approximated ambient temperature values are also illustrated as a basis for comparison with the own measured values. As already observed in the Cu–Zn system, the difference between the depicted Raoult line and the zinc activity values is reduced with increasing temperature. At ambient temperature as well as at  $1000^\circ\text{C}$ , a huge change of the activity values is observed at equimolar composition. After adopting the high-temperature values to ambient-temperature, the activity values are in good agreement with the values from literature.

## 2.5. EMF Measurements on Intermetallic ZnPt Electrodes

EMF measurements were also conducted on single-phase ZnPt electrodes. Figure 7 shows the corresponding time-dependent potential profiles of  $\text{Zn}_{44.2}\text{Pt}_{55.8}$ ,  $\text{Zn}_{49.5}\text{Pt}_{50.5}$  and  $\text{Zn}_{50.4}\text{Pt}_{49.6}$ . The disturbances of the equilibrium by polishing during the EMF measurements are again indicated by arrows. The more platinum-rich intermetallic ZnPt electrodes  $\text{Zn}_{44.2}\text{Pt}_{55.8}$  and  $\text{Zn}_{49.5}\text{Pt}_{50.5}$  already show a stable and reproducible potential value ( $\text{Zn}_{44.2}\text{Pt}_{55.8} = 756.4(5)$  mV,  $\text{Zn}_{49.5}\text{Pt}_{50.5} = 510(2)$  mV) within 30 minutes after the beginning of the EMF measurements. In contrast, the zinc-rich  $\text{Zn}_{50.4}\text{Pt}_{49.6}$  shows an asymptotic potential drop after the beginning of the EMF measurement, which leads to a stable and also reproducible potential value of 113.7(8) mV after about four hours. As in the case of ZnPd, compositions with more than 50% precious metal approach their equilibrium potentials from lower potential values, Zn-rich compositions from higher potential values.

ZnPt tends to show the same qualitative composition-dependent change in the equilibrium potentials as ZnPd. The potential profiles during the adjustment of equilibrium, which differ depending on the elemental composition, are comparable in both systems and can therefore be attributed to an intrinsic effect. It is conceivable, for example, that the initial potentials of the electrodes obtained before the start of an equilibrium adjustment are similar for each measurement. Depending on the equilibrium potential to be achieved, an approximation would then be expected based on a relatively higher or lower potential value to be considered. The initial duration of several hours until the equilibrium value is set at  $\text{Zn}_{50.4}\text{Pt}_{49.6}$  is probably due to an experimental effect. In this case, the distance between the embedded electrodes in the electrolyte and the vessel wall was unintentionally too small, which led to an inhibition of diffusion and a slower adjustment of the equilibrium. This assumption is strengthened by the fact that the equilibrium range could be reached much faster again after disturbance of equilibrium and subsequent reorientation of the embedded electrodes in the electrolyte vessel (around 3.75 h in Figure 7).

The zinc activity values resulting from the equilibrium potentials for  $\text{Zn}_{44.2}\text{Pt}_{55.8}$  ( $\ln a_{\text{Zn}} = -58.91(4)$ ),  $\text{Zn}_{49.5}\text{Pt}_{50.5}$  ( $\ln a_{\text{Zn}} = -39.7(1)$ ) and  $\text{Zn}_{50.4}\text{Pt}_{49.6}$  ( $\ln a_{\text{Zn}} = -8.86(6)$ ) are illustrated in

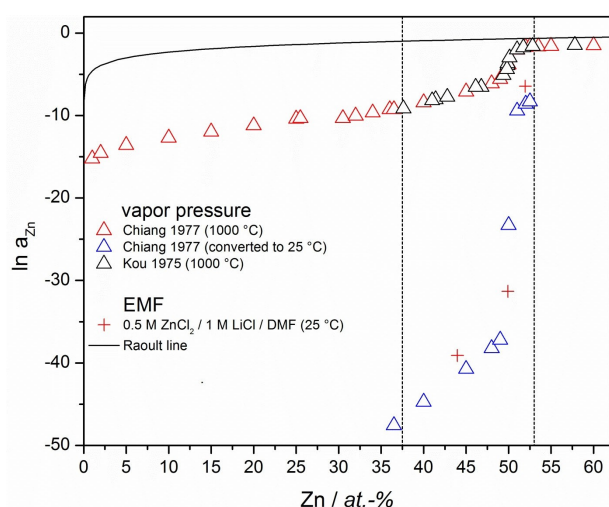


**Figure 6.** Zinc activity values of the Pd–Zn system plotted against atomic percentage of zinc.<sup>[51,52]</sup> The standard deviations of the own measured values lie within the plotted symbols. The homogeneity range of the intermetallic compound ZnPd at  $900^\circ\text{C}$  is indicated by dashed lines.

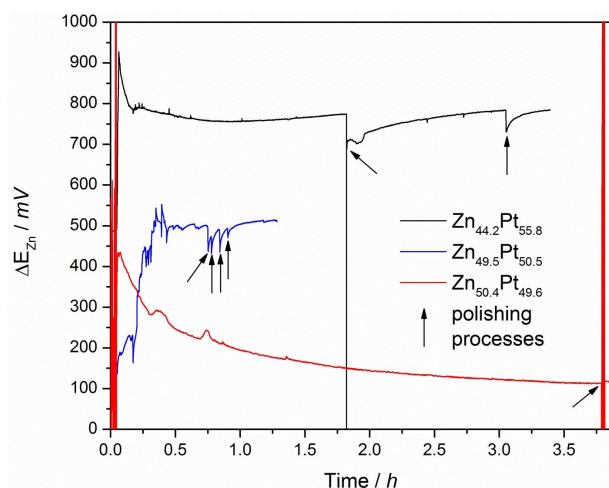


**Figure 7.** EMF measurements on  $\text{Zn}_{44.2}\text{Pt}_{55.8}$ ,  $\text{Zn}_{49.5}\text{Pt}_{50.5}$  and  $\text{Zn}_{50.4}\text{Pt}_{49.6}$  in inert gas atmosphere by using  $0.5\text{ M ZnCl}_2/1\text{ M LiCl}/\text{DMF}$  as electrolyte. In each case the electrode surfaces were renewed before the measurements were started.



Figure 8. Comparison to literature values, determined at 1000 °C, reveals a strong deviation of the zinc activity values from the ideal behavior with decreasing temperature. These two phenomena are (as already explained for the binary Cu–Zn system) lead back to the increase of the interatomic interactions with a decrease of the temperature and a dominance of the bonding interactions between atoms of different element types. Furthermore, at 1000 °C as well as at ambient temperature, a strong activity gradient can be recognized within the homogeneity range of ZnPt, which is (analogous to the homogeneity range of ZnPd) in the area of equimolar composition. A direct comparison of the determined zinc activity values with values of comparable elementary composition converted to ambient temperature is unfortunately not possible due to a lack of partial zinc enthalpies within the thermodynamic data. However, it can be observed that zinc activity values converted to ambient temperature with 64 at.-% zinc result in the same order of magnitude as the zinc activity value determined for the  $\text{Zn}_{50.4}\text{Pt}_{49.6}$  electrode.

Thus, the obtained values and their variation with composition appear meaningful in comparison to literature data and confirm the assumption that equilibrium states can be achieved in the course of the EMF investigations at ambient temperature under inert conditions.

### 3. Conclusion

Corrosion-free EMF measurements were carried out after the development of a corresponding measurement methodology, which especially is characterized by the handling of samples (electrodes) in an inert gas atmosphere, the use of an anhydrous electrolyte and the generation of fresh electrode surfaces before starting the measurements. The correctness of the obtained EMF values was confirmed by comparison to reference data for well-studied  $\text{Cu}_5\text{Zn}_8$  electrodes. The composi-

tion-dependent EMF measurements carried out on intermetallic ZnPd and ZnPt electrodes represent the first thermodynamic studies of these compounds at ambient temperature. The evaluation of the obtained data shows an abrupt change of the zinc activity values of ZnPd and ZnPt at their equimolar composition. The observed change of the zinc activity values of ZnPd and ZnPt is consistent with results of earlier vapor pressure studies on ZnPd and ZnPt conducted at 750 to 1000 °C. The methodology can be applied to any conducting material, thus offering a quantitative material development in terms of tailoring the chemical stability for the application in question.

### Acknowledgements

The authors thank J. Grin for his unfathomable support especially during the move from the MPI CPFS in Dresden to the Technical University Chemnitz. Furthermore, we acknowledge P. Schmidt and H. Ipser for providing valuable input regarding thermodynamic issues. We thank T. Breitenborn for the assistance during the construction of the polishing device.

### Conflict of Interest

The authors declare no conflict of interest.

**Keywords:** determination of activity values, electromotive force, intermetallic compounds, potential measurement, thermodynamic data

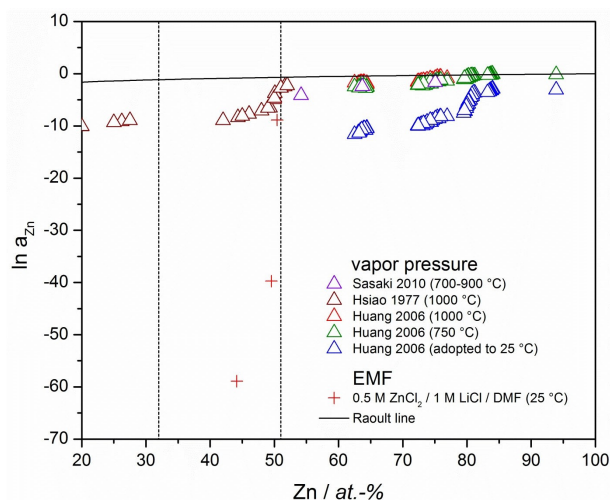


**Figure 8.** Zinc activity values of the Pt–Zn system plotted against atomic percentage of zinc.<sup>[53–55]</sup> The homogeneity range of the intermetallic compound ZnPt at 900 °C is indicated by dashed lines.

- [1] R. Schlögl, *Angew. Chem. Int. Ed.* **2015**, *54*, 3465–3520; *Angew. Chem.* **2015**, *127*, 3531–3589.
- [2] R. Potyrailo, K. Rajan, K. Stoewe, I. Takeuchi, B. Chisholm, H. Lam, *ACS Comb. Sci.* **2011**, *13*, 579–633.
- [3] K. D. Collins, T. Gensch, F. Glorius, *Nat. Chem.* **2014**, *6*, 859–871.
- [4] M. Armbrüster, R. Schlögl, Y. Grin, *Sci. Technol. Adv. Mater.* **2014**, *15*, 034803.
- [5] O. Matselko, R. R. Zimmermann, A. Ormeci, U. Burkhardt, R. Gladyshevskii, Y. Grin, M. Armbrüster, *J. Phys. Chem. C* **2018**, *122*, 21891–21896.
- [6] M. Armbrüster, K. Kovnir, M. Friedrich, D. Teschner, G. Wowsnick, M. Hahne, P. Gille, L. Szentmiklósi, M. Feuerbacher, M. Heggen, F. Girgsdies, D. Rosenthal, R. Schlögl, Y. Grin, *Nat. Mater.* **2012**, *11*, 690–693.
- [7] C. Ziegler, S. Klosz, L. Borchardt, M. Oschatz, S. Kaskel, M. Friedrich, R. Kriegel, T. Keilhauer, M. Armbrüster, A. Eychmüller, *Adv. Funct. Mater.* **2016**, *26*, 1014–1020.
- [8] L. Röbner, M. Armbrüster, *ACS Catal.* **2019**, *9*, 2018–2062.
- [9] M. Friedrich, S. Penner, M. Heggen, M. Armbrüster, *Angew. Chem. Int. Ed.* **2013**, *52*, 4389–4392; *Angew. Chem.* **2013**, *125*, 4485–4488.
- [10] J. Xu, X. Su, X. Liu, P. Xiaoli, G. Pei, Y. Huang, X. Wang, T. Zhang, H. Geng, *Applied Catalysis A* **2016**, *514*, 51–59.
- [11] M. W. Tew, H. Emerich, J. A. van Bokhoven, *J. Phys. Chem. C* **2011**, *115*, 8457–8465.
- [12] Y. Yang, W. Xiao, X. Feng, Y. Xiong, M. Gong, T. Shen, Y. Lu, H. D. Abruña, D. Wang, *ACS Nano* **2019**, *13*, 5968–5974.
- [13] J. Hagen, *Technische Katalyse*, Wiley-VCH, Weinheim, **2008**.
- [14] J. N. Brönsted, *Chem. Rev.* **1928**, *5*, 231–338.
- [15] M. G. Evans, M. Polanyi, *Trans. Faraday Soc.* **1938**, *34*, 11–23.
- [16] F. Abild-Pedersen, J. Greeley, F. Studt, J. Rossmeisl, T. R. Munter, P. G. Moses, E. Skúlason, T. Bligaard, J. K. Nørskov, *Phys. Rev. Lett.* **2007**, *99*, 016105.

- [17] P. Schmidt, Habilitation, Technische Universität Dresden, 2007.
- [18] J. Cheng, P. Hu, *Angew. Chem. Int. Ed.* **2011**, *50*, 7650–7654; *Angew. Chem.* **2011**, *123*, 7792–7796.
- [19] A. Mikula, *JOM.* **2007**, *59*, 35–37.
- [20] H. A. Laitinen, W. S. Ferguson, R. A. Osteryoung, *J. Electrochem. Soc.* **1957**, *104*, 516–520.
- [21] J. N. Pratt, *Metall. Trans. A.* **1990**, *21*, 1223–1250.
- [22] O. Kubaschewski, E. L. Evans, *Metallurgische Thermochemie*, VEB Verlag Technik, Berlin, 1959.
- [23] G. Schwitzgebel, *Chem. Ing. Tech.* **1974**, *46*, 169–169.
- [24] G. Schwitzgebel, J. Lang, R. Sass, *Z. Phys. Chem.* **1985**, *146*, 87–96.
- [25] G. Schwitzgebel, *Z. Phys. Chem.* **1975**, *95*, 15–24.
- [26] G. Schwitzgebel, *Acta Metall.* **1972**, *20*, 1297–1303.
- [27] D. C. A. Ivarsson, U. Burkhardt, K. Richter, R. Kriegel, L. Rößner, M. Neumann, M. Armbrüster, *J. Alloys Compd.* **2018**, *743*, 155–162.
- [28] in EC-Lab (Version 11.01), Bio-Logic - Science Instruments, City, 2016.
- [29] M. Armand, F. Endres, D. R. MacFarlane, H. Ohno, B. Scrosati, *Nat. Mater.* **2009**, *8*, 621–629.
- [30] M. Galiński, A. Lewandowski, I. Stępnik, *Electrochim. Acta.* **2006**, *51*, 5567–5580.
- [31] N. De Vos, C. Maton, C. V. Stevens, *ChemElectroChem.* **2014**, *1*, 1258–1270.
- [32] J. Both, *IEEE Electr. Insul. Mag.* **2015**, *31*, 24–34.
- [33] F. Tambornino, J. Sappl, F. Pultar, T. M. Cong, S. Hübner, T. Giftthaler, C. Hoch, *Inorg. Chem.* **2016**, *55*, 11551–11559.
- [34] N. David, J. M. Fiorani, M. Vilasi, J. Hertz, *J. Phase Equilib.* **2003**, *24*, 240–248.
- [35] A. Ölander, *Z. Phys. Chem.* **1933**, *164*, 428–438.
- [36] O. J. Kleppa, C. E. Thalmayer, *J. Phys. Chem.* **1959**, *63*, 1953–1958.
- [37] T. C. Wilder, W. E. Galin, *Trans. Metall. Soc. AIME.* **1969**, *245*, 1287–1290.
- [38] T. B. Massalski, *Binary Alloy Phase Diagrams*, ASM International, Ohio, 1990.
- [39] J. P. Pemsler, E. J. Rapperport, *Trans. Metall. Soc. AIME.* **1969**, *245*, 1395–1400.
- [40] C. Cunat, J. Hertz, *C. R. Seances Acad. Sci., Ser. C.* **1977**, *285*, 183–185.
- [41] E. J. Rapperport, J. P. Pemsler, *Metall. Trans.* **1972**, *3*, 827–831.
- [42] C. E. Birchenall, R. F. Mehl, *Trans. Am. Inst. Min. Metall. Pet. Eng.* **1947**, *171*, 143–165.
- [43] A. W. Herbenar, C. A. Siebert, O. S. Duffendack, *Trans. Am. Inst. Min. Metall. Pet. Eng.* **1950**, *188*, 323–326.
- [44] A. Schneider, H. Schmid, *Z. Elektrochem. Angew. Phys. Chem.* **1942**, *48*, 627–639.
- [45] B. B. Argent, D. W. Wakeman, *Trans. Faraday Soc.* **1958**, *54*, 799–806.
- [46] D. B. Masson, J.-L. Sheu, *Metall. Trans.* **1970**, *1*, 3005–3009.
- [47] L. H. Everett, P. W. M. Jacobs, J. A. Kitchener, *Acta Metall.* **1957**, *5*, 281–284.
- [48] D. B. Downie, *Acta Metall.* **1964**, *12*, 875–882.
- [49] E. B. Koklyanov, E. B. Kritskaya, G. P. Miroevskii, B. P. Burylev, L. S. Tsemekhman, *Russ. J. Appl. Chem.* **2003**, *76*, 714–718.
- [50] D. R. Gaskell, *Introduction to the Thermodynamics of Materials*, Taylor & Francis Group, New York/London, 2008.
- [51] T. H. Chiang, H. Ipser, Y. A. Chang, *Z. Metallkd.* **1977**, *68*, 141–147.
- [52] S. Kou, Y. A. Chang, *Acta Metall.* **1975**, *23*, 1185–1190.
- [53] Y. J. Hsiao, Y. A. Chang, H. Ipser, *J. Electrochem. Soc.* **1977**, *124*, 1235–1239.
- [54] H. Sasaki, T. Nagai, M. Maeda, *J. Alloys Compd.* **2010**, *504*, 475–478.
- [55] Y. Z. Huang, K. W. Richter, W. X. Yuan, Z. Y. Qiao, H. Ipser, *Int. J. Mater. Res.* **2006**, *97*, 429–433.

---

Manuscript received: December 24, 2019  
Revised manuscript received: February 10, 2020  
Accepted manuscript online: March 24, 2020  
Version of record online: April 7, 2020